A general search for new phenomena in *ep* scattering at HERA

H1 Collaboration

A. Aktas [k], V. Andreev [aa], T. Anthonis [d,e], A. Asmone [ah], A. Babaev [z], S. Backovic [al],
J. Bähr [al], P. Baranov [aa], E. Barrelet [ae], W. Bartel [k], S. Baumgartner [am], J. Becker [an],
M. Beckingham [v], O. Behnke [n], O. Behrendt [h], A. Belousov [aa], Ch. Berger [a],
N. Berger [am], T. Berndt [o], J.C. Bizot [ac], J. Böhme [k], M.-O. Boenig [h], V. Boudry [ad],
J. Bracinik [ab], V. Brisson [ac], H.-B. Bröker [b], D.P. Brown [k], D. Bruncko [q], F.W. Büsser [l],
A. Bunyatyan [m,ak], G. Buschhorn [ab], L. Bystritskaya [z], A.J. Campbell [k], S. Caron [a],
F. Cassol-Brunner [w], K. Cerny [ag], V. Chekelian [ab], J.G. Contreras [x], Y.R. Coppens [c],
J.A. Coughlan [f], B.E. Cox [v], G. Cozzika [j], J. Cvach [af], J.B. Dainton [s], W.D. Dau [p],
K. Daum [aj,1], B. Delcourt [ac], R. Demirchyan [ak], A. De Roeck [k,2], K. Desch [l],
E.A. De Wolf [d,e], C. Diaconu [w], J. Dingfelder [n], V. Dodonov [m,✠], A. Dubak [ab],
C. Duprel [b], G. Eckerlin [k], V. Efremenko [z], S. Egli [ai], R. Eichler [ai], F. Eisele [n],
M. Ellerbrock [n], E. Elsen [k], M. Erdmann [k,3], W. Erdmann [am], P.J.W. Faulkner [c],
L. Favart [d,e], A. Fedotov [z], R. Felst [k], J. Ferencei [k], M. Fleischer [k], P. Fleischmann [k],
Y.H. Fleming [k], G. Flucke [k], G. Flügge [b], A. Fomenko [aa], I. Foresti [an], J. Formánek [ag],
G. Franke [k], G. Frising [a], E. Gabathuler [s], K. Gabathuler [ai], E. Garutti [k], J. Garvey [c],
J. Gayler [k], R. Gerhards [k,✠], C. Gerlich [n], S. Ghazaryan [ak], S. Ginzburgskaya [z],
L. Goerlich [g], N. Gogitidze [aa], S. Gorbounov [al], C. Grab [am], H. Grässler [b], T. Greenshaw [s],
M. Gregori [t], G. Grindhammer [ab], C. Gwilliam [v], D. Haidt [k], L. Hajduk [g], J. Haller [n],
M. Hansson [u], G. Heinzelmann [l], R.C.W. Henderson [r], H. Henschel [al], O. Henshaw [c],
G. Herrera [y], I. Herynek [af], R.-D. Heuer [l], M. Hildebrandt [ai], K.H. Hiller [al], P. Höting [b],
D. Hoffmann [w], R. Horisberger [ai], A. Hovhannisyan [ak], M. Ibbotson [v], M. Ismail [v],
M. Jacquet [ac], L. Janauschek [ab], X. Janssen [k], V. Jemanov [l], L. Jönsson [u], D.P. Johnson [d,e],
H. Jung [u,k], D. Kant [t], M. Kapichine [i], M. Karlsson [u], J. Katzy [k], N. Keller [an],
J. Kennedy [s], I.R. Kenyon [c], C. Kiesling [ab], M. Klein [al], C. Kleinwort [k], T. Klimkovich [k],
T. Kluge [a], G. Knies [k], A. Knutsson [u], B. Koblitz [ab], V. Korbel [k], P. Kostka [al],
R. Koutouev [m], A. Kropivnitskaya [z], J. Kroseberg [an], K. Krüger [o], J. Kückens [k],
T. Kuhr [k], M.P.J. Landon [t], W. Lange [al], T. Laštovička [al,ag], P. Laycock [s], A. Lebedev [aa],
B. Leißner [a], R. Lemrani [k], V. Lendermann [o], S. Levonian [k], L. Lindfeld [an], K. Lipka [al],

B. List [am], E. Lobodzinska [al,g], N. Loktionova [aa], R. Lopez-Fernandez [k], V. Lubimov [z],
H. Lueders [l], D. Lüke [h,k], T. Lux [l], L. Lytkin [m], A. Makankine [i], N. Malden [v],
E. Malinovski [aa], S. Mangano [am], P. Marage [d,e], J. Marks [n], R. Marshall [v],
M. Martisikova [k], H.-U. Martyn [a], S.J. Maxfield [s], D. Meer [am], A. Mehta [s], K. Meier [o],
A.B. Meyer [l], H. Meyer [aj], J. Meyer [k], S. Mikocki [g], I. Milcewicz-Mika [g], D. Milstead [s],
A. Mohamed [s], F. Moreau [ad], A. Morozov [i], I. Morozov [i], J.V. Morris [f], M.U. Mozer [n],
K. Müller [an], P. Murín [q,4], V. Nagovizin [z], K. Nankov [k], B. Naroska [l], J. Naumann [h],
Th. Naumann [al], P.R. Newman [c], C. Niebuhr [k], A. Nikiforov [ab], D. Nikitin [i], G. Nowak [g],
M. Nozicka [ag], R. Oganezov [ak], B. Olivier [k], J.E. Olsson [k], G. Ossoskov [i], D. Ozerov [z],
A. Paramonov [z], C. Pascaud [ac], G.D. Patel [s], M. Peez [ad], E. Perez [j], A. Perieanu [k],
A. Petrukhin [z], D. Pitzl [k], R. Plačakytė [ab], R. Pöschl [k], B. Portheault [ac], B. Povh [m],
N. Raicevic [al], P. Reimer [af], B. Reisert [ab], A. Rimmer [s], C. Risler [ab], E. Rizvi [c],
P. Robmann [an], B. Roland [d,e], R. Roosen [d,e], A. Rostovtsev [z], Z. Rurikova [ab],
S. Rusakov [aa], K. Rybicki [g,✠], D.P.C. Sankey [f], E. Sauvan [w], S. Schätzel [n], J. Scheins [k],
F.-P. Schilling [k], P. Schleper [k], S. Schmidt [ab], S. Schmitt [an], M. Schneider [w],
L. Schoeffel [j], A. Schöning [am], V. Schröder [k], H.-C. Schultz-Coulon [o],
C. Schwanenberger [k], K. Sedlák [af], F. Sefkow [k], I. Sheviakov [aa], L.N. Shtarkov [aa],
Y. Sirois [ad], T. Sloan [r], P. Smirnov [aa], Y. Soloviev [aa], D. South [k], V. Spaskov [i],
A. Specka [ad], H. Spitzer [l], R. Stamen [k], B. Stella [ah], J. Stiewe [o], I. Strauch [k],
U. Straumann [an], V. Tchoulakov [i], G. Thompson [t], P.D. Thompson [c], F. Tomasz [o],
D. Traynor [t], P. Truöl [an], G. Tsipolitis [k,5], I. Tsurin [al], J. Turnau [g], E. Tzamariudaki [ab],
A. Uraev [z], M. Urban [an], A. Usik [aa], D. Utkin [z], S. Valkár [ag], A. Valkárová [ag], C. Vallée [w],
P. Van Mechelen [d,e], N. Van Remortel [d,e], A. Vargas Trevino [h], Y. Vazdik [aa], C. Veelken [s],
A. Vest [a], S. Vinokurova [k], V. Volchinski [ak], K. Wacker [h], J. Wagner [k], G. Weber [l],
R. Weber [am], D. Wegener [h], C. Werner [n], N. Werner [an], M. Wessels [a], B. Wessling [l],
G.-G. Winter [k], Ch. Wissing [h], E.-E. Woehrling [c], R. Wolf [n], E. Wünsch [k], S. Xella [an],
W. Yan [k], V. Yeganov [ak], J. Žáček [ag], J. Zálešák [af], Z. Zhang [ac], A. Zhelezov [z],
A. Zhokin [z], H. Zohrabyan [ak], F. Zomer [ac]

[a] *I. Physikalisches Institut der RWTH, Aachen, Germany* [6]
[b] *III. Physikalisches Institut der RWTH, Aachen, Germany* [6]
[c] *School of Physics and Astronomy, University of Birmingham, Birmingham, UK* [7]
[d] *Inter-University Institute for High Energies ULB-VUB, Brussels*
[e] *Universiteit Antwerpen, Antwerpen, Belgium* [8]
[f] *Rutherford Appleton Laboratory, Chilton, Didcot, UK* [7]
[g] *Institute for Nuclear Physics, Cracow, Poland* [9]
[h] *Institut für Physik, Universität Dortmund, Dortmund, Germany* [6]
[i] *Joint Institute for Nuclear Research, Dubna, Russia*
[j] *CEA, DSM/DAPNIA, CE-Saclay, Gif-sur-Yvette, France*
[k] *DESY, Hamburg, Germany*
[l] *Institut für Experimentalphysik, Universität Hamburg, Hamburg, Germany* [6]
[m] *Max-Planck-Institut für Kernphysik, Heidelberg, Germany*

[n] *Physikalisches Institut, Universität Heidelberg, Heidelberg, Germany* [6]

[o] *Kirchhoff-Institut für Physik, Universität Heidelberg, Heidelberg, Germany* [6]

[p] *Institut für Experimentelle und Angewandte Physik, Universität Kiel, Kiel, Germany*

[q] *Institute of Experimental Physics, Slovak Academy of Sciences, Košice, Slovak Republic* [10,11]

[r] *Department of Physics, University of Lancaster, Lancaster, UK* [7]

[s] *Department of Physics, University of Liverpool, Liverpool, UK* [7]

[t] *Queen Mary and Westfield College, London, UK* [7]

[u] *Physics Department, University of Lund, Lund, Sweden* [12]

[v] *Physics Department, University of Manchester, Manchester, UK* [7]

[w] *CPPM, CNRS/IN2P3, Univ Mediterranee, Marseille, France*

[x] *Departamento de Fisica Aplicada, CINVESTAV, Mérida, Yucatán, Mexico* [15]

[y] *Departamento de Fisica, CINVESTAV, Mexico* [15]

[z] *Institute for Theoretical and Experimental Physics, Moscow, Russia* [16]

[aa] *Lebedev Physical Institute, Moscow, Russia* [10]

[ab] *Max-Planck-Institut für Physik, München, Germany*

[ac] *LAL, Université de Paris-Sud, IN2P3-CNRS, Orsay, France*

[ad] *LLR, Ecole Polytechnique, IN2P3-CNRS, Palaiseau, France*

[ae] *LPNHE, Universités Paris VI and VII, IN2P3-CNRS, Paris, France*

[af] *Institute of Physics, Academy of Sciences of the Czech Republic, Praha, Czech Republic* [10,13]

[ag] *Faculty of Mathematics and Physics, Charles University, Praha, Czech Republic* [10,13]

[ah] *Dipartimento di Fisica Università di Roma Tre and INFN Roma 3, Roma, Italy*

[ai] *Paul Scherrer Institut, Villigen, Switzerland*

[aj] *Fachbereich Physik, Bergische Universität Gesamthochschule Wuppertal, Wuppertal, Germany*

[ak] *Yerevan Physics Institute, Yerevan, Armenia*

[al] *DESY, Zeuthen, Germany*

[am] *Institut für Teilchenphysik, ETH, Zürich, Switzerland* [14]

[an] *Physik-Institut der Universität Zürich, Zürich, Switzerland* [14]

Abstract

A model-independent search for deviations from the Standard Model prediction is performed in e^+p and e^-p collisions at HERA using H1 data corresponding to an integrated luminosity of 117 pb^{-1}. For the first time all event topologies involving isolated electrons, photons, muons, neutrinos and jets with high transverse momenta are investigated in a single analysis. Events are assigned to exclusive classes according to their final state. A statistical algorithm is developed to search for deviations from the Standard Model in the distributions of the scalar sum of transverse momenta or invariant mass of final state particles and to quantify their significance. A good agreement with the Standard Model prediction is observed in most of the event classes. The most significant deviation is found for a topology containing an isolated muon, missing transverse momentum and a jet, consistent with a previously reported observation.
© 2004 Elsevier B.V. All rights reserved.

1. Introduction

At HERA electrons[12] and protons collide at a centre-of-mass energy of up to 319 GeV. These high-energy electron-proton interactions provide a testing ground for the Standard Model (SM) complementary to e^+e^- and $p\bar{p}$ scattering. It is widely believed that the SM is incomplete and that new physics signals may appear below energies of 1 TeV. Many extensions to the SM have been constructed during the last decades predicting various phenomena which may be visible at high energies or large transverse momenta (P_T). HERA data have been used to test some of these models of new processes by analysing their anticipated experimental signatures and limits on their parameters have been derived [1].

The approach described in this Letter consists of a comprehensive and generic search for deviations from the SM prediction at large transverse momenta. All high P_T final state configurations involving electrons (e), muons (μ), jets (j), photons (γ) or neutrinos (ν) are systematically investigated.[13] The analysis covers phase space regions where the SM prediction is sufficiently precise to detect anomalies and does not rely on assumptions concerning the characteristics of any SM extension. Such a model-independent approach might discover unexpected manifestations of new physics. Therefore it addresses the important question of whether evidence for new physics might still be hidden in the high P_T data recorded at collider experiments. A similar strategy for a model-independent search was previously presented in [2].

All final states containing at least two objects (e, μ, j, γ, ν) with $P_T > 20$ GeV in the polar angle[14] range $10° < \theta < 140°$ are investigated. The complete HERA I data sample (1994–2000) is used, corresponding to an integrated luminosity of 117 pb^{-1}. All selected events are classified into exclusive event classes according to the number and types of objects detected in the final state (e.g., e–j, μ–j–ν, j–j–j–j–j). These exclusive event classes ensure a clear separation of final states and allow an unambiguous statistical interpretation of deviations. All experimentally accessible combinations of objects have been studied and data events are found in 22 of them.

In a first analysis step the global event yields of the event classes are compared with the SM expectation. The distributions of the invariant mass M_{all} and of the scalar sum of transverse momenta $\sum P_T$ of high P_T final state objects are presented. New physics may be visible as an excess or a deficit in one of these distributions. Therefore, in a second step these distributions are systematically investigated using a dedicated algorithm which locates the region with the largest deviation of the data from the SM prediction. The probability of occurrence of such a deviation is derived, both

---

[12] In this Letter "electrons" refers to both electrons and positrons, if not otherwise stated.

[13] The analysis covers objects which can be well identified in the H1 detector for all final state configurations. Since the selection efficiencies and purities for τ leptons and beauty quarks are rather low, these particles are not treated as explicit objects.

[14] The origin of the H1 coordinate system is the nominal ep interaction point, with the direction of the proton beam defining the positive z-axis (forward region). The transverse momenta are measured in the xy plane. The pseudorapidity η is related to the polar angle θ by $\eta = -\ln\tan(\theta/2)$.

for each event class individually and globally for all classes combined.

This Letter is organised as follows. Section 2 describes the Standard Model processes at HERA and their Monte Carlo simulation. The H1 detector, the event selection and measurement procedure are described in Section 3. The event yields and distributions for each event class are presented in Section 4. The search strategy and results are explained in Section 5. Section 6 summarises the Letter.

2. Standard Model processes and Monte Carlo generation

Several Monte Carlo event generators are combined to simulate events for all SM processes which have large cross sections or are expected to be dominant for specific event classes, avoiding double-counting. The data sets used for the development of the Monte Carlo generators are largely independent of the events in the current analysis. All processes are generated with an integrated luminosity significantly higher than that of the data sample and events are passed through a full detector simulation [3]. At high transverse momenta the dominant SM processes are the photoproduction of two jets and neutral current (NC) deep-inelastic scattering (DIS). In the following the abbreviation X represents all reaction products other than the high P_T objects considered.

Photoproduction of jets and photons. To simulate the direct and resolved photoproduction of jets $ep \rightarrow jjX$, prompt photon production $ep \rightarrow \gamma jX$ and the resolved photoproduction of photon pairs $ep \rightarrow \gamma \gamma X$, the PYTHIA 6.1 event generator [4] is used. Light and heavy flavoured jets are generated. The simulation contains the Born level hard scattering matrix elements and radiative QED corrections.

Neutral current deep-inelastic scattering. The Born, QCD Compton and Boson Gluon Fusion matrix elements are used in the RAPGAP [5] event generator to model NC DIS events. The QED radiative effects arising from real photon emission from both the incoming and the outgoing electrons are simulated using the HERACLES [6] generator. Hence the NC DIS prediction contains the processes $ep \rightarrow ejX$, $ep \rightarrow ejjX$ and also models final states with an additional radiated photon.

Charged current deep-inelastic scattering. Charged current (CC) DIS events are simulated using the DJANGO [7] program, which includes first order QED radiative corrections based on HERACLES. This prediction contributes to the final states $ep \rightarrow \nu jX$, $ep \rightarrow \nu jjX$ and to final states with an additional radiated photon.

QED Compton scattering. Elastic and quasi-elastic Compton processes $ep \rightarrow e\gamma X$ are simulated with the WABGEN [9] generator. The inelastic contribution is already included in the NC DIS RAPGAP sample.

Electroweak production of lepton pairs. Multi-lepton events (ee, $\mu\mu$, $\tau\tau$) are generated with the GRAPE [10] program, which includes all electroweak matrix elements at tree level. Multilepton production via $\gamma\gamma$, γZ, ZZ collisions, internal photon conversion and the decay of virtual or real Z bosons is considered. Initial and final state QED radiation is included. The complete hadronic final state is obtained via interfaces to PYTHIA and SOPHIA [11] for the inelastic and quasi-elastic regimes, respectively.

W production. The production of W bosons $ep \rightarrow WX$ and $ep \rightarrow WjX$ is modelled using EPVEC [12]. Next-to-leading order QCD corrections [13] are taken into account by reweighting the events as a function of the transverse momentum and rapidity of the W boson [14].

Processes with the production of three or more jets, e.g., $ep \rightarrow jjjX$ or $ep \rightarrow jjjjX$, are accounted for using leading logarithmic parton showers as a representation of higher order QCD radiation, with the exception of CC DIS, where the colour-dipole model [8] is used. Hadronisation is modelled using Lund string fragmentation [4]. The prediction of processes with two or more high transverse momentum jets, e.g., $ep \rightarrow jjX$, $ep \rightarrow ejjX$, is scaled by a factor of 1.2 to normalise the leading order Monte Carlos to next-to-leading order QCD calculations [15].

3. Experimental technique

3.1. The H1 detector

The H1 detector [16] components relevant to the present analysis are briefly described here. Jets, photons and electrons are measured with the Liquid Argon (LAr) calorimeter [17], which covers the polar angle range $4° < \theta < 154°$ with full azimuthal acceptance. Electromagnetic shower energies are measured with a precision of $\sigma(E)/E = 12\%/\sqrt{E/\text{GeV}} \oplus 1\%$ and hadronic energies with $\sigma(E)/E = 50\%/\sqrt{E/\text{GeV}} \oplus 2\%$, as measured in test beams. The central and forward tracking detectors are used to measure charged particle trajectories, to reconstruct the interaction vertex and to supplement the measurement of the hadronic energy. The innermost proportional chamber CIP ($9° < \theta < 171°$) is used to veto charged particles for the identification of photons. The LAr and inner tracking detectors are enclosed in a superconducting magnetic coil with a strength of 1.15 T. The return yoke of the coil is the outermost part of the detector and is equipped with streamer tubes forming the central muon detector ($4° < \theta < 171°$). It is also used to supplement the measurement of hadrons. In the forward region of the detector ($3° < \theta < 17°$) a set of drift chamber layers (the forward muon system) detects muons and, together with an iron toroidal magnet, allows a momentum measurement. The luminosity measurement is based on the Bethe–Heitler process $ep \rightarrow ep\gamma$, where the photon is detected in a calorimeter [18] located downstream of the interaction point.

The main trigger for events with high transverse momentum is provided by the LAr calorimeter. The trigger efficiency is close to 100% for events having an electromagnetic deposit in the LAr (electron or photon) with transverse momentum greater than 20 GeV [19]. Events triggered only by jets have a trigger efficiency above 90% for $P_T^{\text{jet}} > 20$ GeV and nearly 100% for $P_T^{\text{jet}} > 25$ GeV [20]. For events with missing transverse momentum above 20 GeV, determined from an imbalance in the transverse momentum measured in the calorimeter, the trigger efficiency is $\sim 90\%$. The muon trigger is based on single muon signatures from the central muon detector, which are combined with signals from the central tracking detector. The trigger efficiency for di-muon events is about 70% [21].

3.2. Event selection

At HERA electrons or positrons with an energy of 27.6 GeV collide with protons at an energy of 920 GeV resulting in a centre-of-mass energy of $\sqrt{s} = 319$ GeV. Before 1998 the proton energy was 820 GeV resulting in a centre-of-mass energy of $\sqrt{s} = 301$ GeV. The event sample studied consists of the full 1994–2000 HERA I data set. It corresponds to an integrated luminosity of 36.4 pb^{-1} in e^+p scattering at $\sqrt{s} = 301$ GeV and 13.8 pb^{-1} in e^-p scattering and 66.4 pb^{-1} in e^+p scattering at $\sqrt{s} = 319$ GeV.

The data selection requires at least one isolated electromagnetic cluster, jet or muon to be found in the detector acceptance. Energy deposits in the calorimeters and tracks in the inner tracking system are used to form combined cluster-track objects, from which the hadronic energy is reconstructed. To reduce background it is demanded that the event vertex be reconstructed within 35 cm in z of the nominal position[15] and that $\sum_i (E_i - P_{z,i}) < 75$ GeV, where E_i is the particle energy and $P_{z,i}$ is the z component of the particle momentum. Here, the index i runs over all hadronic energy deposits, electromagnetic clusters and muons found in the event. Due to energy-momentum conservation events are expected to have a value of $\sum_i (E_i - P_{z,i}) = 55.2$ GeV, twice the electron beam energy, if only longitudinal momentum along the proton beam direction is unmeasured. Events with topologies typical of cosmic ray and beam-induced background are rejected [22]. Moreover, the timing of the event is required to coincide with that of the ep bunch crossing.

The identification criteria for each type of particle are based on those applied in previous analyses of specific final states [15,19,21,23]. Additional requirements are chosen to ensure an unambiguous identification of particles, whilst retaining high efficiencies. The following paragraphs describe the identification criteria for the different objects and give the identification

---

[15] This is not required for the event classes containing only photons or photons and a neutrino.

efficiencies for the kinematic region considered in the analysis.

Electron identification. The electron identification is based on the measurement of a compact and isolated electromagnetic shower in the LAr calorimeter. The hadronic energy within a distance in the pseudorapidity-azimuth $(\eta - \phi)$ plane $R = \sqrt{(\Delta\eta)^2 + (\Delta\phi)^2} < 0.75$ around the electron is required to be below 2.5% of the electron energy. This calorimetric electron identification is complemented by tracking conditions. A high quality track is required to geometrically match the electromagnetic cluster within a distance of closest approach to the cluster centre-of-gravity of 12 cm. No other good track is allowed within $R < 0.5$ around the electron direction. In the central region $(20° < \theta < 140°)$ the distance between the first measured point in the central drift chambers and the beam axis is required to be below 30 cm in order to reject photons that convert late in the central tracker material. In addition, the transverse momentum measured from the associated track $P_T^{e_{tk}}$ is required to match the calorimetric measurement P_T^e with $1/P_T^{e_{tk}} - 1/P_T^e < 0.02$ GeV^{-1}. In the region not fully covered by the central drift chambers $(10° < \theta < 37°)$ a wider isolation cone of $R = 1$ is required to reduce the contribution of fake electrons from hadrons. In this forward region the identification is completed by the requirement of associated hits in the CIP, which reduces the contamination from neutral particles showering in the material of the forward region. The resulting electron finding efficiency is 85% in the central region and 70% in the forward region.

Photon identification. The photon identification relies on the measurement of an electromagnetic shower and on the same calorimetric isolation criteria against hadrons as for the electron identification. In addition, photons are required to be separated from jets with $P_T^{\text{jet}} > 5$ GeV by a distance of $R > 1$ to the jet axis. Vetoes are applied on any charged track pointing to the electromagnetic cluster. No track should be present with a distance of closest approach to the cluster below 24 cm or within $R < 0.5$. An additional veto on any hits in the CIP is applied. The resulting photon identification efficiency as derived using elastic QED Compton events is 90%.

Muon identification. The muon identification is based on a track in the forward muon system or in the inner tracking systems associated with a track segment or an energy deposit in the central muon detector [23]. The muon momentum is measured from the track curvature in the toroidal or solenoidal magnetic fields. A muon candidate should have no more than 8 GeV deposited in the LAr calorimeter in a cylinder of radius 0.5 in $(\eta - \phi)$ space, centred on the muon track direction. In di-muon events, the requirement of an opening angle between the two muons smaller than 165° discards cosmic ray background. Beam halo muons are rejected by requiring that the muons originate from the event vertex. Finally, misidentified hadrons are almost completely suppressed by requiring that the muon candidate is separated from the closest jet with $P_T^{\text{jet}} > 5$ GeV by $R > 1$. The efficiency to identify muons is greater than 90% [23].

Jet identification. Jets are defined using the inclusive $k_\perp$ algorithm [24,25]. The algorithm is applied in the laboratory frame with a separation parameter of 1 and using a P_T weighted recombination scheme [24] in which the jets are treated as massless. The jet algorithm is run on all combined cluster-track objects not previously identified as electron or photon candidates. The scattered electron may fake a jet. This effect is important for multi-jet events, especially at high transverse momenta. To reject these fake jets, the first radial moment of the jet transverse energy [26,27] is required to be greater than 0.02 and the quantity $M^{\text{jet}}/P_T^{\text{jet}}$ must be greater than 0.1 [15,27]. The invariant mass M^{jet} is obtained using the four-vector of all objects belonging to the jet. If the fraction of the jet energy contained in the electromagnetic part of the LAr calorimeter is greater than 0.9, the above criteria are tightened to 0.04 and 0.15, respectively. The jet selection efficiency is 97%.

Neutrino identification. A neutrino candidate is defined in events with missing transverse momentum above 20 GeV. The missing momentum is derived from all identified particles and energy deposits in the event. Fake missing transverse momentum may also arise from the mismeasurement of an identified object. This effect is reduced by requiring that

the neutrino[16] be isolated from all identified objects with a transverse momentum above 20 GeV. Requiring $\sum_i (E_i - P_{z,i}) < 48$ GeV discards neutrino candidates from NC processes where the missing transverse momentum is caused by energy leakage in the forward region. If exactly one electron or muon object is found, a neutrino object is only assigned to an event if $\Delta\phi(l - X_{tot}) < 170°$, where $\Delta\phi(l - X_{tot})$ is the separation in azimuthal angle between the lepton l and the direction of the system X_{tot} built of all hadronic energies.

Event classification. The common phase space for electrons, photons, muons and jets is defined by $10° < \theta < 140°$ and $P_T > 20$ GeV. The neutrino phase space is defined by missing transverse momentum above 20 GeV and $\sum_i (E_i - P_{z,i}) < 48$ GeV. These values are chosen to retain a high selection and trigger efficiency. All particles with $P_T > 20$ GeV, including the neutrino defined by its reconstructed four-vector, are required to be isolated compared with each other by a minimum distance R of one unit in the $\eta - \phi$ plane. The events are classified, depending on the number and types of objects, into exclusive event classes. Events with an isolated calorimetric object in the considered phase space which is not identified as a photon, electron or jet are discarded from the analysis in order to minimise wrong classifications.

Based on these identification criteria, purities can be derived for each event class with a sizeable SM expectation. Purity is defined as the ratio of SM events reconstructed in the event class in which they are generated to the total number of reconstructed events in this class. Most purities are found to be above 60% and they are close to 100% for the j–j, e–j, j–ν and μ–μ event classes.

3.3. Systematic uncertainties

This section describes the sources of experimental and theoretical systematic uncertainties considered. Experimental systematic uncertainties arising from the measurement of the objects are listed in Table 1 (for more details see [20,27,28]).

---

[16] The four-vector of the neutrino is calculated under the assumption $\sum_i (E_i - P_{z,i}) + (E_\nu - P_{z,\nu}) = 55.2$ GeV.

Table 1
Systematic uncertainties attributed to the measurement of energies and polar angles and to the identification efficiencies of particles

Object	Energy scale	θ (mrad)	Identification efficiency
Jet	2%	5–10	–
Electron	0.7–3%	1–3	2–7%
Photon	0.7–3%	1–3	2–7%
Muon	5%	3	5%

- The electromagnetic energy scale uncertainty varies between 0.7% and 3% depending on the particle's impact point on the LAr calorimeter surface [19]. The polar angular measurement uncertainty of electromagnetic clusters varies depending on θ between 1 and 3 mrad [19]. The identification of electron and photon candidates depends on the tracking efficiency, which is known with a precision ranging from 2% for polar angles above $37°$ to 7% in the forward region.
- The hadronic energy scale of the LAr calorimeter is known to 2%. The uncertainty on the jet polar angle determination is 5 mrad for $\theta < 30°$ and 10 mrad for $\theta > 30°$.
- The uncertainty on the transverse momentum measurement for muons amounts to 5%. The uncertainty on the polar angle is 3 mrad. The muon identification efficiency is known with a precision of 5%.
- The trigger uncertainties for each class are determined by the object with the highest trigger efficiency. The uncertainty on the trigger efficiency is estimated to be 3% if the event is triggered by a jet or missing transverse momentum and 5% if it is triggered by a muon. For electrons and photons the uncertainty on the trigger efficiency is negligible.
- The uncertainty in the integrated luminosity results in an overall normalisation error of 1.5%.
- The uncertainty in the reconstruction of $\sum_i (E_i - P_{z,i})$ and the missing P_T for the neutrino classification are obtained by propagation of the systematic errors for other objects.

Depending on the generator level production process, different theoretical uncertainties are used as listed in Table 2. The errors attributed to the predictions for $ep \to jjX$, $ep \to j\gamma X$, $ep \to j\nu X$, $ep \to$

Table 2
Theoretical uncertainties attributed to the simulation of different SM processes

Process	Uncertainty
$ep \to jjX$ and $ep \to j\gamma X$	15%
$ep \to j\nu X$ and $ep \to jeX$	10%
$ep \to jj\nu X$ and $ep \to jjeX$	15%
$ep \to \mu\mu X$ and $ep \to eeX$	3%
$ep \to WX$ and $ep \to WjX$	15%
$ep \to e\gamma X$ and $ep \to e\gamma j$	10%
$ep \to e\gamma p$	5%

jeX, $ep \to jj\nu X$, $ep \to jjeX$ and W production include uncertainties in the parton distribution functions and those due to missing higher order corrections [15,23,27,28]. The error attributed to $ep \to \mu\mu X$ and $ep \to eeX$ results mainly from the limited knowledge of the proton structure [21,29]. The error on the QED Compton cross section is estimated to be 5% for elastic and 10% for inelastic production. An additional theoretical error of 20% is applied for each jet produced by parton shower processes (e.g., 20% for the $j-j-j$ event class). An uncertainty of 50% is added to the prediction for NC DIS events with missing transverse momentum above 20 GeV and a high P_T electron. This uncertainty is estimated by a comparison of the missing transverse momentum distribution between NC DIS events with a low P_T electron ($P_T < 20$ GeV) and the SM prediction.

All systematic errors are added in quadrature and are assigned to the SM predictions. For example, the resulting total uncertainties for $e-j$ events are 10% and 35% at low (50 GeV) and high (250 GeV) invariant mass M_{all}, respectively. In the $j-j$ event class the errors are typically 20% and reach 40–50% for M_{all} and $\sum P_T$ values around 250 GeV.

4. Event yields

All possible event classes with at least two objects are investigated.[17] The event yields subdivided into event classes are presented for the data and SM ex-

---

[17] The $\mu-\nu$ event class is discarded from the present analysis. It is dominated by low transverse energy photoproduction events in which a poorly reconstructed muon gives rise to missing transverse momentum, which fakes the neutrino signature.
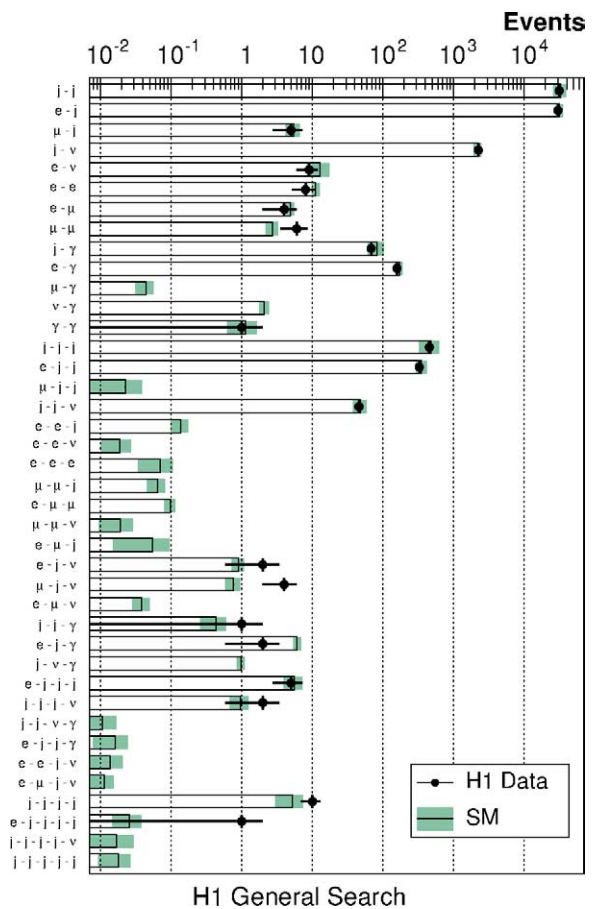

Fig. 1. The data and the SM expectation for all event classes with a SM expectation greater than 0.01 events. The analysed data sample corresponds to an integrated luminosity of 117 pb^{-1}. The error bands on the predictions include model uncertainties and experimental systematic errors added in quadrature.

pectation in Fig. 1. All event classes with a SM expectation greater than 0.01 events are shown. No other event class contains data events. The distributions of the scalar sum of transverse momenta $\sum P_T$ and of the invariant mass M_{all} of all objects are presented in Figs. 2 and 3 for classes with at least one event.

The dominant high P_T processes at HERA, i.e., photoproduction of jets, NC and CC DIS, dominate in the $j-j$, $e-j$ and $j-\nu$ event classes, respectively. Events are observed with $\sum P_T$ and M_{all} values as large as 250 GeV. A good description of the data spectra by the prediction is observed. The prediction for the event classes $j-j-\gamma$ and $e-j-\gamma$ is dominated by photoproduction and NC DIS processes with the radiation
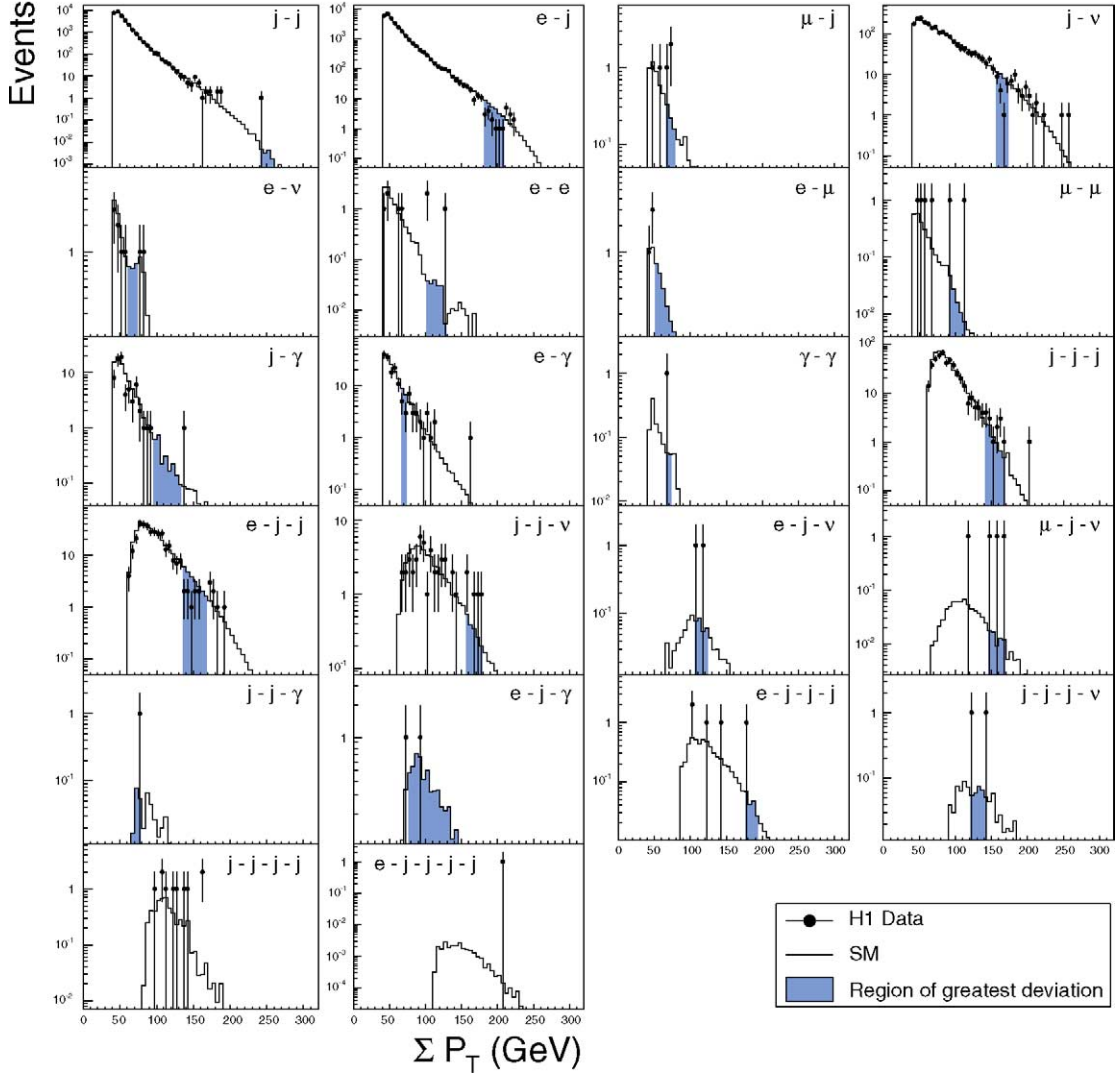
H1 General Search - $\Sigma\, P_T$ Distributions

Fig. 2. The number of data events and the SM expectation as a function of $\sum P_T$ for classes with at least one event. The shaded areas show the regions of greatest deviation chosen by the search algorithm. No search is performed for the j–j–j–j and e–j–j–j classes.

of a photon, respectively. There is good agreement between the data and the prediction. No event is observed in the radiative CC classes ν–γ and j–ν–γ, consistent with the expectation of 2.1 ± 0.3 and 1.0 ± 0.1, respectively. The j–j–j, e–j–j, e–j–j–j, j–j–ν and j–j–j–ν event classes correspond to processes with additional jet production due to higher order QCD radiation. The yields of these event classes are also well described by the SM prediction.

The e–γ event class is dominated by QED Compton scattering processes and $\sum P_T$ and $M_{\rm all}$ values up to 160 GeV are measured. A good agreement with the SM is observed. The prompt photon j–γ event class extends up to $M_{\rm all} \sim 150$ GeV and is well described by the prediction. The purity in this class is moderate (40–50%) due to the high background from misidentified electrons in NC DIS. Backgrounds where hadrons are misidentified as photons are small. One event is
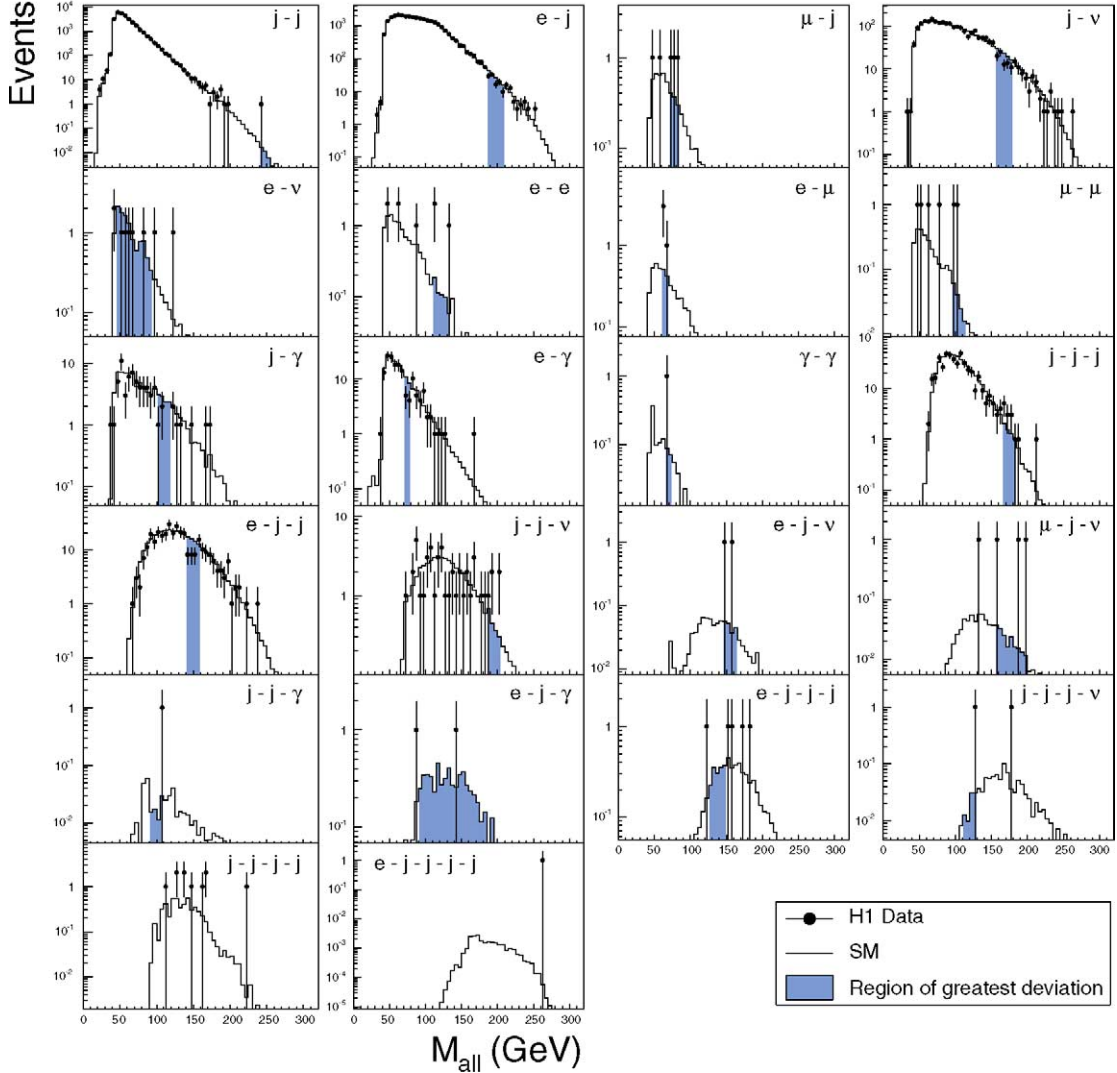
H1 General Search - M_{all} Distributions

Fig. 3. The number of data events and the SM expectation as a function of M_{all} for event classes with at least one event. The shaded areas show the regions of greatest deviation chosen by the search algorithm. No search is performed for the $j–j–j–j$ and $e–j–j–j–j$ classes.

observed in the $\gamma–\gamma$ event class for an expectation of 1.1 ± 0.5, which is dominated by the $ep \rightarrow e\gamma X$ process, where the electron is misidentified. Contributions of higher order QED processes, which could lead to two high transverse momentum photons, are negligible.

Lepton pair production from $\gamma\gamma$ processes dominates in event classes with several leptons. The $e–e$ event class contains 8 events for an expectation of

11.2 ± 1.4. In this channel, a discrepancy with the SM expectation was previously reported for high masses by the H1 Collaboration [29]. All multi-electron events mentioned in [29] and located in the phase space of this analysis are found. In the region $M_{all} > 100$ GeV, 3 events are observed and 1.16 ± 0.25 are expected. The higher SM prediction compared with the prediction of 0.3 in [29] is due to the extended polar angle range in the forward re-

gion. This leads to an additional ≈ 0.4 background events from fake electrons and ≈ 0.4 events from the $ep \rightarrow eeX$ processes. The e–e–e class contains no events. None of the tri-electron events of [29] are selected here due to the requirement of high transverse momentum. The predictions for the e–μ and μ–μ event classes are dominated by muon pair production from two-photon reactions. The e–μ event class is populated if the scattered electron and only one of the muons are selected. In the e–μ class, 4 events are observed compared with an expectation of 4.8 ± 0.6. A slight excess is observed in the μ–μ event class where 6 events are found and 2.7 ± 0.6 are expected. Muon pair production processes also contribute $\approx 85\%$ in the μ–j event class, where a good agreement is found. In the e–μ, μ–μ and μ–j event classes the $\sum P_T$ and M_{all} values of the data lie between 50 and 100 GeV.

The prediction for the event classes μ–j–ν and e–j–ν consists mainly of high P_T W production with a subsequent leptonic decay. A discrepancy between the data and the SM expectation is observed in the μ–j–ν event class, where 4 events are observed for an expectation of 0.8 ± 0.2. The $\sum P_T$ values reach 170 GeV and the M_{all} values 200 GeV. In this event class less than 0.002 background events are expected from the photoproduction of jets via QCD processes. Such a deviation was previously reported in [23] and will be further discussed in Section 5. In the e–j–ν event class 2 data events are observed for an expectation of 0.9 ± 0.2. Some of the e–j–ν events mentioned in [23] have an electron with a transverse momentum below 20 GeV and are therefore not selected as e–j–ν events in the present analysis. The event topology e–ν is also expected to contain events arising from W production together with background from NC DIS. In the e–ν event class, 9 data events are observed compared with an expectation of 12.9 ± 4.5.

A slight excess of the data compared with the prediction is observed in the j–j–j–j event class, with 10 data events observed and 5.2 ± 2.2 expected. One event is observed in the e–j–j–j–j event class, to be compared with an expectation of 0.026 ± 0.011. This event has a $\sum P_T$ of 207 GeV and an invariant mass M_{all} of 262 GeV. The NC DIS expectation for $M_{\text{all}} > 260$ GeV is $(9 \pm 6) \times 10^{-5}$ as derived using RAP-GAP. The energy flow of the event in the $\eta - \phi$ view is presented in Fig. 4. The NC DIS and photoproduc-
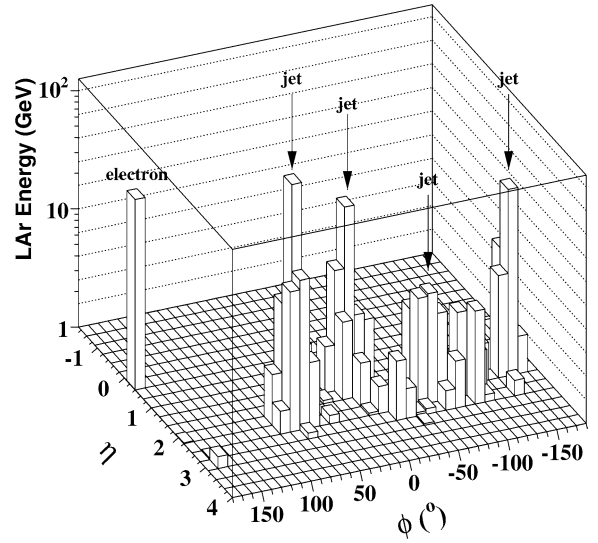

Fig. 4. The calorimetric energy deposits of the e–j–j–j–j event as a function of η and ϕ.

tion SM predictions have been tested using a sample of j–j–j–j events with $P_T^{\text{jet}} > 15$ GeV and e–j–j–j–j events with $P_T^e > 10$ GeV and $P_T^{\text{jet}} > 5$ GeV. An adequate description of the $\sum P_T$ and M_{all} distributions of the data is obtained within the quoted SM uncertainties. Since the NC DIS prediction for $M_{\text{all}} > 260$ GeV is only of order 0.001 fb, rare SM processes not considered in this analysis such as W pair production may be dominant in this kinematic domain.

No events are found in any other event class, in agreement with the SM expectation (see Fig. 1).

5. Search for deviations from the Standard Model

5.1. Search algorithm and strategy

In order to quantify the level of agreement between the data and the SM expectation and to identify regions of possible deviations, a new search algorithm is developed. Detailed studies have shown that M_{all} and $\sum P_T$ have a large sensitivity to new physics (see appendix and [28]). The algorithm described in the following locates the region of largest deviation of the data from the SM in these distributions. The calculation of the significance of this deviation is inspired by [2].

Definition of regions. A region in the $\sum P_T$ and M_{all} distributions is defined as a set of connected histogram bins[18] with a size of at least twice the resolution. All possible regions of any width and at any position in the histograms are considered. The number of data events (N_{obs}), the SM expectation (N_{SM}) and its total systematic uncertainty (δN_{SM}) are calculated for each region.

Determination of the most interesting region. A statistical estimator p is defined to judge which region is of most interest. This estimator is derived from the convolution of the Poisson probability density function (pdf) to account for statistical errors with a Gaussian pdf, $G(b; N_{\mathrm{SM}}, \delta N_{\mathrm{SM}})$, with mean N_{SM} and width δN_{SM}, to include the effect of non-negligible systematic uncertainties. The estimator is defined via

$$
p = \begin{cases}
A \int_0^\infty db\, G(b; N_{\mathrm{SM}}, \delta N_{\mathrm{SM}}) \\
\times \sum_{i=N_{\mathrm{obs}}}^\infty \frac{e^{-b} b^i}{i!} \\
\quad \text{if } N_{\mathrm{obs}} \geqslant N_{\mathrm{SM}}, \\
A \int_0^\infty db\, G(b; N_{\mathrm{SM}}, \delta N_{\mathrm{SM}}) \\
\times \sum_{i=0}^{N_{\mathrm{obs}}} \frac{e^{-b} b^i}{i!} \\
\quad \text{if } N_{\mathrm{obs}} < N_{\mathrm{SM}}
\end{cases}
$$

$$
\text{with } A = 1 \Big/ \left[\int_0^\infty db\, G(b; N_{\mathrm{SM}}, \delta N_{\mathrm{SM}}) \sum_{i=0}^\infty \frac{e^{-b} b^i}{i!} \right].
$$

The factor A ensures normalisation to unity. If G is replaced by a Dirac delta function $\delta(b - N_{\mathrm{SM}})$ the estimator p becomes the usual Poisson probability. The value of p gives an estimate of the probability of a fluctuation of the SM expectation upwards (downwards) to at least (at most) the observed number of data events in the region considered. The region of greatest deviation is the region having the smallest p-value, $p_{\min}$. Such a method is able to find narrow resonances and single outstanding events as well as signals spread over large regions of phase space in distributions of any shape [28].

Significance per event class. The probability that a fluctuation with a p-value at least as small as $p_{\min}$ oc-

---

[18] In order to minimise binning effects, a bin size smaller than or comparable with the resolution of the studied quantity is used. A 5 GeV bin size is used for all distributions. Further reduction of the bin size has a negligible effect on the results.

curs anywhere in the distribution is estimated using the following method. Many independent hypothetical data histograms are made by filling each bin with an event number diced according to the pdfs of the SM expectation (again a convolution of Poisson and Gaussian pdfs). For each of these hypothetical data histograms the algorithm is run to find the region of greatest deviation and the corresponding $p_{\min}^{\mathrm{SM}}$ is calculated. The probability $\hat{P}$ is then defined as the fraction of hypothetical data histograms with a $p_{\min}^{\mathrm{SM}}$ equal to or smaller than the $p_{\min}$ value obtained from the data. $\hat{P}$ is a measure of the statistical significance of the deviation observed in the data. If the event classes are exclusive, the $\hat{P}$ values can be used to compare the results of different event classes. Depending on the final state, a $p_{\min}$-value of 5.7×10^{-7} ("5σ") corresponds to a value of $-\log_{10} \hat{P}$ between 5 and 6.

Global significance. The overall degree of agreement with the SM can be further quantified by taking into account the large number of event classes studied in this analysis. The probability of observing an event class with a given $\hat{P}$ value or smaller can be calculated with Monte Carlo (MC) experiments. A MC experiment is defined as a set of hypothetical data histograms (either in M_{all} or in $\sum P_T$) following the SM expectation with an integrated luminosity of $117\,\mathrm{pb}^{-1}$, on which the complete search algorithm and statistical analysis are applied as for data. This procedure is repeated many times. The expectation for the $\hat{P}$ values observed in the data is then given by the distribution of $\hat{P}^{\mathrm{SM}}$ values obtained from all MC experiments. The probability to find a $\hat{P}$ value smaller than the minimum observed in the data can thus be calculated and quantifies the global significance of the observed deviation.

5.2. Search results

The final $\hat{P}$ values obtained for event classes having at least one observed event are summarised in Table 3. The regions selected by the algorithm are presented in Figs. 2 and 3.

The most significant deviation of the analysis is found in the μ–j–ν event class. This class has $\hat{P}$ values of 0.010 (M_{all}) and 0.001 ($\sum P_T$). The mass region ($155 < M_{\mathrm{all}} < 200$ GeV) contains 3 data events for an expectation of 0.19 ± 0.05. In the chosen $\sum P_T$ region ($145 < \sum P_T < 170$ GeV) three data events are

Table 3

The $\hat{P}$ values, the number of data events N_{obs} and the SM expectation N_{SM} for the region derived by the search algorithm using the M_{all} and $\sum P_T$ distributions for event classes containing at least one event and taken into account in the statistical procedure. The p value in the selected region is also presented

Event class	M_{all}					$\sum P_T$				
	$\hat{P}$	N_{obs}	N_{SM}	$\pm\delta N_{\mathrm{SM}}$	p	$\hat{P}$	N_{obs}	N_{SM}	$\pm\delta N_{\mathrm{SM}}$	p
j–j	0.38	1	0.035	±0.017	0.036	0.12	1	0.013	±0.006	0.013
e–j	0.94	111	139	±21	0.12	0.021	12	31.2	±5.1	0.0028
μ–j	0.67	3	1.07	±0.25	0.098	0.29	3	0.70	±0.23	0.040
j–ν	0.34	83	116	±14	0.028	0.22	20	36.7	±6.2	0.023
e–ν	0.94	5	10.6	±4.4	0.17	0.77	0	2.1	±0.8	0.17
e–e	0.32	3	0.56	±0.17	0.023	0.019	3	0.18	±0.08	0.0013
e–μ	0.21	4	0.93	±0.12	0.016	0.56	0	2.6	±0.5	0.080
μ–μ	0.069	2	0.14	±0.04	0.010	0.036	2	0.11	±0.03	0.0060
j–γ	0.52	3	10.8	±3.7	0.052	0.77	0	2.5	±1.0	0.13
e–γ	0.38	9	19.2	±2.0	0.014	0.64	8	15.7	±1.9	0.040
γ–γ	0.47	1	0.16	±0.09	0.15	0.31	1	0.11	±0.09	0.12
j–j–j	0.41	12	5.9	±2.0	0.050	0.58	14	7.8	±2.5	0.077
e–j–j	0.69	39	59.6	±10.7	0.058	0.085	9	23.9	±4.4	0.0072
j–j–ν	0.62	5	1.79	±0.41	0.043	0.51	5	1.74	±0.45	0.040
e–j–ν	0.090	2	0.19	±0.05	0.016	0.16	2	0.28	±0.06	0.034
μ–j–ν	9.7×10^{-3}	3	0.19	±0.05	0.0011	1.0×10^{-3}	3	0.068	±0.029	7.5×10^{-5}
j–j–γ	0.27	1	0.074	±0.048	0.076	0.36	1	0.15	±0.10	0.15
e–j–γ	0.47	1	5.7	±1.6	0.050	0.39	1	5.6	±1.4	0.045
e–j–j–j	0.98	0	1.6	±0.5	0.23	0.87	1	0.18	±0.06	0.17
j–j–j–ν	0.33	1	0.084	±0.045	0.083	0.20	2	0.31	±0.14	0.044

found while only 0.07 ± 0.03 are expected. This event topology was studied in [23] where this deviation at high P_T was already reported.

A $\hat{P}$ value of 0.019 is found in the e–e event class in a region at high transverse momenta, $100 < \sum P_T < 130$ GeV where 3 events are observed for an expectation of 0.18 ± 0.08. The deviation is less prominent in the region selected in the invariant mass distribution due to a higher background from NC DIS events. This corresponds to the excess of data events also identified in [29].

A deficit is observed in the e–j event class in the $\sum P_T$ distribution in the region $180 < \sum P_T < 210$ GeV. For a SM expectation of 31.2 ± 5.0 only 12 data events are observed. The derived $\hat{P}$ value is 0.021.

Due to the uncertainties in the SM prediction in the j–j–j–j and e–j–j–j–j event classes at the highest M_{all} and $\sum P_T$, where data events are observed (see Section 4), no reliable $\hat{P}$ values can be calculated for these classes. Consequently, these event classes are not taken into account to determine the overall degree of agreement between the data and the SM.

The $\hat{P}$ values for event classes with no data event observed and a small SM expectation are 1. This remains the case if an additional contribution is added from a possible further rare process not included here. Such classes can thus be considered in the calculation of the global significance.

The $\hat{P}$ values observed in the data in all event classes are compared in Fig. 5 with the distribution of $\hat{P}^{\mathrm{SM}}$ obtained from the large set of MC experiments, normalised to one experiment. The comparison is presented for the scans of the M_{all} and $\sum P_T$ distributions. Most $\hat{P}$ values lie above 0.01, corresponding to event classes where no significant discrepancy between the data and the SM expectation is observed. The global probabilities to find at least one class with a $\hat{P}$ value smaller than the observation in the μ–j–ν channel are 3 and 28% for the $\sum P_T$ and M_{all} distributions, respectively (see Appendix A for details).

To test the dependence of the analysis on the *a priori* defined P_T cuts, the whole analysis is repeated with two other object P_T cuts. The P_T cut was raised to 40 GeV for all objects and lowered to 15 GeV. In the latter case it was still required that at least one
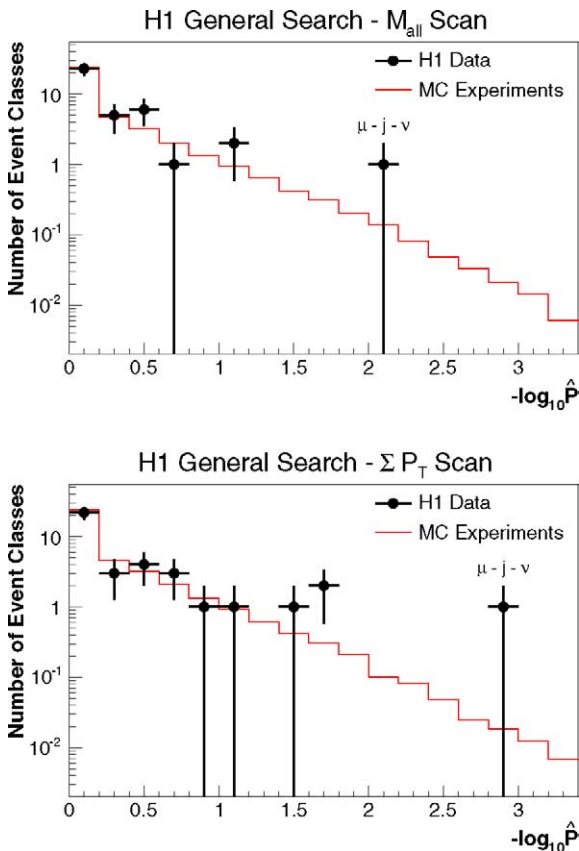
Fig. 5. The $-\log_{10} \hat{P}$ values for the data event classes and the expected distribution from MC experiments, as derived by investigating the M_{all} distributions (top) and $\sum P_T$ distributions (bottom) with the search algorithm.

object has a P_T larger than 20 GeV in order to maintain a high trigger efficiency. The analysis was also repeated separately on the $e^+ p$ and $e^- p$ data samples. In these four test scenarios a similar overall agreement with the SM is observed. The $\mu–j–\nu$ event class remains the one with the smallest $\hat{P}$ value in the scenario with a lowered P_T cut in the $e^+ p$ data sample and no new discrepancy is observed. When raising the P_T cut to 40 GeV, it is mainly the two particle event classes containing jets that are still populated and the largest deviation is observed in the $e–e$ class with $\hat{P} = 0.01$.

6. Conclusions

The data collected with the H1 experiment during the years 1994–2000 (HERA I) have been investi-gated in a search for deviations from the SM prediction at high transverse momentum. For the first time all event topologies involving isolated electrons, photons, muons, neutrinos and jets are investigated in a single analysis. Many event clases are studied for the first time at HERA, others are re-investigated in an extended kinematic regime and with the full HERA I luminosity. A good agreement between the data and the SM expectation is found in most event classes. A better knowledge of rare processes may be required to search for deviations from the SM in final states with four jets at the highest invariant mass or trans-verse momentum. The distributions in the invariant mass and scalar sum of transverse momenta of the particles in each event class have been systematically searched for deviations using a statistical algorithm. The most significant deviation is found in the $\mu–j–\nu$ event class, a topology where deviations have also been previously reported. About 3% (28%) of hypo-thetical Monte Carlo experiments would produce a deviation in at least one event class which is more sig-nificant than that observed in the corresponding sum of transverse momenta (invariant mass) distribution of the topology with a jet, a muon and a neutrino.

Acknowledgements

Appendix A

Signals for new physics may appear either as a single deviation or a small set of deviations. The fol-lowing outlines how a significant deviation might be defined and presents tests of the sensitivity of this analysis to specific signals for new physics.

The probability P_X^n to observe in the data a

Table 4
The probability P_X^n to find at least n event classes with a $-\log \hat{P}$ value greater than X. The values are applicable to both the M_{all} and $\sum P_T$ analyses

n	P_1	$P_{1.5}$	P_2	$P_{2.5}$	P_3	$P_{3.5}$	P_4	$P_{4.5}$	P_5
1	95%	65%	28%	9%	3%	0.9%	0.2%	0.1%	$< 0.05\%$
2	79%	28%	4%	0.6%	0.1%	$< 0.05\%$	–	–	–
3	53%	8%	0.4%	0.05%	$< 0.05\%$	–	–	–	–

$-\log_{10} \hat{P}$ greater than X in at least n event classes is given by the fraction of MC experiments having at least n event classes with a $-\log_{10} \hat{P}^{\text{SM}} > X$. The P_X^n values obtained for this analysis are presented in Table 4. Up to 3 event classes are considered. Since very similar P_X^n values are found for the M_{all} and $\sum P_T$ distributions, averaged values are presented. For example, a P_X^n value smaller than 0.0005, which might be considered to represent a significant deviation, could be obtained from one event class with a $-\log_{10} \hat{P} > 5$, two event classes with a $-\log_{10} \hat{P} > 3.5$ or three event classes with a $-\log_{10} \hat{P} > 3$. It was found that one of these cases occurs either in M_{all} or $\sum P_T$ in around 0.1% of all MC experiments.

A set of pseudo data samples has been produced to test the sensitivity of the analysis procedure to some dedicated signals for new physics. The prediction of a specific model for new physics is added to the SM prediction and this new total prediction is used to generate pseudo data samples. Again a Monte Carlo technique is used to vary the distribution of signal events and generate many MC experiments. The complete algorithm is run on those MC experiments and the mean value of $-\log_{10} \hat{P}$ in all of them is derived as a measure of sensitivity of this analysis.

The exotic production of top quarks via a flavour-changing neutral current is first investigated. The decay $t \to bW$ with subsequent leptonic and hadronic W decays has been considered. The $\langle -\log_{10} \hat{P} \rangle$ values obtained are displayed in Fig. 6 (top) as a function of the cross section for producing a top when the proton beam energy is 920 GeV. Whereas $\langle -\log_{10} \hat{P} \rangle$ is around 0.43 if no signal is present, the value increases if a top is produced. In the $j–j–j$ event class a $\langle -\log_{10} \hat{P} \rangle$ of 2 is obtained for a cross-section σ_{top} of ~ 0.5 pb. This value can be compared with the 95% confidence level exclusion limit on the top production cross section at $\sigma_{\text{top}} < 0.48$ pb already derived by the H1 experiment using the hadronic top decay channel only [30]. A deviation with three event classes with a
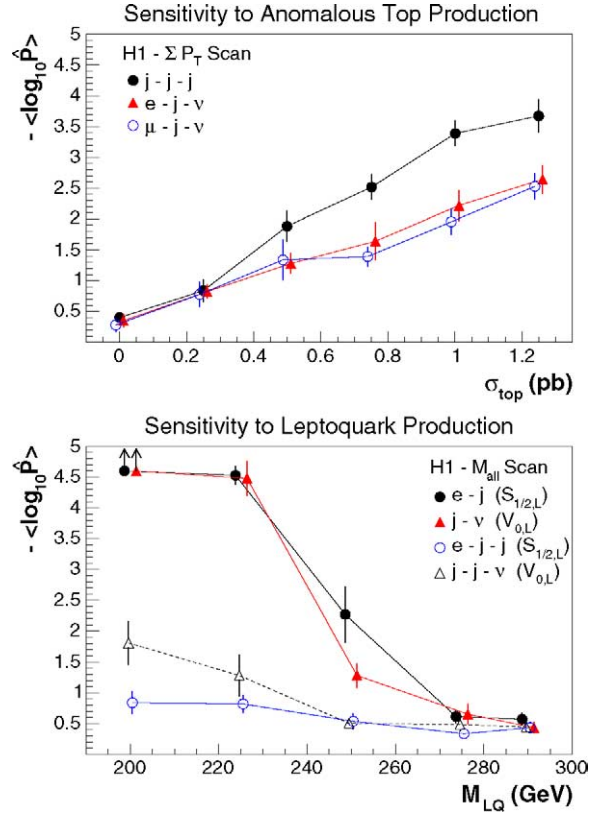

Fig. 6. The mean value of $-\log_{10} \hat{P}$ as derived from MC experiments which include a top signal with a cross section σ_{top} (top) and a LQ signal with a mass M_{LQ} and a λ coupling equal to 0.05 (bottom), using the distributions of $\sum P_T$ and M_{all}, respectively. The small arrows on the bottom figure indicate that these values should be treated as lower limits.

$\langle -\log_{10} \hat{P} \rangle > 3$ would be found in this example for $\sigma_{\text{top}} \approx 1.5$ pb.

The second test concerns the production of leptoquarks (LQs) [31]. $S_{1/2,L}$ and $V_{0,L}$ type leptoquarks have been considered, which would mainly manifest themselves in the $e–j$ and $j–\nu$ channels. A λ coupling of 0.05 has been assumed and the sensitivity of the present analysis was tested for various LQ masses.

The $\langle -\log_{10} \hat{P} \rangle$ values obtained from searches in the M_{all} distributions are summarised in Fig. 6 (bottom), for both the $S_{1/2,L}$ and $V_{0,L}$ LQ appearing in the $e-j$ and $e-j-j$ as well as the $j-\nu$ and $j-j-\nu$ channels, respectively. This analysis is sensitive to both types of leptoquarks up to masses of 240–250 GeV. These values can be compared with 95% confidence level limits of 265 GeV for $S_{1/2,L}$ LQs and 240 GeV for $V_{0,L}$ LQs, determined by dedicated analyses [32]. As for the case of single top production, the general search is thus found to have a sensitivity to leptoquark production which is comparable with that of dedicated searches.

References

[1] M. Kuze, Y. Sirois, Prog. Part. Nucl. Phys. 50 (2003) 1, hep-ex/0211048.

[2] B. Abbott, et al., D0 Collaboration, Phys. Rev. D 62 (2000) 092004, hep-ex/0006011;
B. Abbott, et al., D0 Collaboration, Phys. Rev. D 64 (2001) 012004, hep-ex/0011067.

[3] R. Brun, F. Bruyant, M. Maire, A.C. McPherson, P. Zanarini, CERN-DD/EE/84-1.

[4] T. Sjöstrand, et al., Comput. Phys. Commun. 135 (2001) 238, hep-ph/0010017, the PARP(67) parameter was set to 4 instead of its default value of 1.

[5] H. Jung, Comput. Phys. Commun. 86 (1995) 147.

[6] A. Kwiatkowski, H. Spiesberger, H.J. Möhring, Comput. Phys. Commun. 69 (1992) 155.

[7] G.A. Schuler, H. Spiesberger, Django: The Interface for The Event Generators Heracles and Lepto.

[8] L. Lönnblad, Comput. Phys. Commun. 71 (1992) 15.

[9] C. Berger, P. Kandel, Prepared for Workshop on Monte Carlo Generators for HERA Physics Hamburg, Germany, 27–30 April 1998.

[10] T. Abe, Comput. Phys. Commun. 136 (2001) 126, hep-ph/0012029.

[11] A. Mucke, et al., Comput. Phys. Commun. 124 (2000) 290, astro-ph/9903478.

[12] U. Baur, J.A. Vermaseren, D. Zeppenfeld, Nucl. Phys. B 375 (1992) 3.

[13] K.P. Diener, C. Schwanenberger, M. Spira, Eur. Phys. J. C 25 (2002) 405, hep-ph/0203269.

[14] K.P. Diener, C. Schwanenberger, M. Spira, hep-ex/0302040.

[15] C. Adloff, et al., H1 Collaboration, Eur. Phys. J. C 25 (2002) 13, hep-ex/0201006.

[16] I. Abt, et al., H1 Collaboration, Nucl. Instrum. Methods A 386 (1997) 348;
I. Abt, et al., H1 Collaboration, Nucl. Instrum. Methods A 386 (1997) 310.

[17] B. Andrieu, et al., H1 Calorimeter Group Collaboration, Nucl. Instrum. Methods A 336 (1993) 460.

[18] R.D. Appuhn, et al., H1 SPACAL Group Collaboration, Nucl. Instrum. Methods A 386 (1997) 397.

[19] C. Adloff, et al., H1 Collaboration, Eur. Phys. J. C 30 (2003) 1, hep-ex/0304003.

[20] M. Peez, Recherche de déviations au Model Standard dans les processus de grande énergie transverse sur le collisionneur électron–proton HERA, Ph.D. Thesis, Université de Lyon, 2003, DESY-THESIS-2003-023, available at http://www-h1.desy.de/psfiles/theses/.

[21] A. Aktas, et al., H1 Collaboration, Phys. Lett. B 583 (2004) 28, hep-ex/0311015.

[22] Z. Zhang, Habilitation Thesis, LAL preprint, LAL 00-57 (2000), hep-ph/0012249.

[23] V. Andreev, et al., H1 Collaboration, Phys. Lett. B 561 (2003) 241, hep-ex/0301030.

[24] S.D. Ellis, D.E. Soper, Phys. Rev. D 48 (1993) 3160, hep-ph/9305266.

[25] S. Catani, Y.L. Dokshitzer, M.H. Seymour, B.R. Webber, Nucl. Phys. B 406 (1993) 187.

[26] W.T. Giele, E.W.N. Glover, D.A. Kosower, Phys. Rev. D 57 (1998) 1878, hep-ph/9706210.

[27] G. Frising, Rare phenomena and W production in electron–proton scattering at HERA, Ph.D. Thesis, RWTH Aachen, 2003, available at http://www-h1.desy.de/psfiles/theses/.

[28] M. Wessels, General search for new phenomena in ep scattering at HERA, Ph.D. Thesis, RWTH Aachen, 2004, available at http://www-h1.desy.de/psfiles/theses/.

[29] A. Aktas, et al., H1 Collaboration, Eur. Phys. J. C 31 (2003) 17, hep-ex/0307015.

[30] A. Aktas, et al., H1 Collaboration, Eur. Phys. J. C 33 (2004) 9, hep-ex/0310032.

[31] C. Adloff, et al., H1 Collaboration, Eur. Phys. J. C 11 (1999) 447, hep-ex/9907002;
C. Adloff, et al., H1 Collaboration, Eur. Phys. J. C 14 (2000) 553, Erratum.

[32] S. Chekanov, et al., ZEUS Collaboration, Phys. Rev. D 68 (2003) 052004, hep-ex/0304008.